

Article

Chloride-Enhanced Removal of Ammonia Nitrogen and Organic Matter from Landfill Leachate by a Microwave/Peroxymonosulfate System

Ke Feng and Qibin Li *

Faculty of Geosciences and Environmental Engineering, Southwest Jiaotong University, Chengdu 611756, China
* Correspondence: liqb@home.swjtu.edu.cn

Abstract: Landfill leachate contains not only high concentrations of refractory organic matter and ammonia nitrogen, but also high concentrations of chloride ions (Cl^-). The modification of reactive species of the peroxymonosulfate (PMS) oxidation system by Cl^- and its priority sequence for the removal of NH_4^+ -N and organic matter from landfill leachate remain unclear. This study investigated the removal characteristics of NH_4^+ -N and organic matter in the microwave (MW)/PMS system with high Cl^- content. The results show that increasing Cl^- concentration significantly improves the production of hypochlorous acid (HOCl) in the MW/PMS system under acidic conditions, and that the thermal and non-thermal effects of MW irradiation have an important influence on the HOCl produced by PMS activation. The maximum cumulative concentration of HOCl was 748.24 μM after a reaction time of 2 min. The formation paths of HOCl are (i) $\text{SO}_4^{\bullet-}$ formed by the MW/PMS system interacting with Cl^- and HO^\bullet , and (ii) the nucleophilic addition reaction of PMS and Cl^- . Moreover, the high concentration of HOCl produced by the system can not only remove NH_4^+ -N in situ, but also interact with PMS to continuously generate Cl^\bullet as an oxidant to participate in the reaction with pollutants (e.g., NH_4^+ -N and organic matter). Common aqueous substances (e.g., CO_3^{2-} , HCO_3^- , NO_3^- , and humic acid) in landfill leachate will compete with NH_4^+ -N for reactive species in the system, and will thereby inhibit its removal to a certain extent. It was found that when NH_4^+ -N and leachate DOM co-exist in landfill leachates, they would compete for reactive species, and that humic acid-like matter was preferentially removed, leading to the retention of fulvic acid-like matter. It is hoped that this study will provide theoretical support for the design and optimization of methods for removing NH_4^+ -N and organic matter from landfill leachate with high chloride ion content.



Citation: Feng, K.; Li, Q. Chloride-Enhanced Removal of Ammonia Nitrogen and Organic Matter from Landfill Leachate by a Microwave/Peroxymonosulfate System. *Catalysts* **2022**, *12*, 1078. <https://doi.org/10.3390/catal12101078>

Academic Editors: Jiangkun Du, Lie Yang and Chengdu Qi

Received: 30 August 2022

Accepted: 17 September 2022

Published: 20 September 2022

Publisher's Note: MDPI stays neutral with regard to jurisdictional claims in published maps and institutional affiliations.



Copyright: © 2022 by the authors. Licensee MDPI, Basel, Switzerland. This article is an open access article distributed under the terms and conditions of the Creative Commons Attribution (CC BY) license (<https://creativecommons.org/licenses/by/4.0/>).

Keywords: peroxymonosulfate; microwave; chloride; ammonia nitrogen; landfill leachate

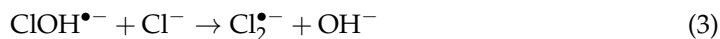
1. Introduction

With the continuous acceleration of urbanization, the output of municipal solid waste is increasing. At the same time, a high volume of secondary pollutants, such as landfill leachate, which contains high concentrations of refractory organic matter, ammonia nitrogen (NH_4^+ -N), chloride ions (Cl^-), and other pollutants, will inevitably be produced [1–8]. Landfill leachate must be properly treated otherwise it will cause a negative impact on the surrounding environment [9]. Advanced oxidation processes (AOPs) based on activated peroxymonosulfate (PMS; HSO_5^-) and peroxydisulfate (PDS; $\text{S}_2\text{O}_8^{2-}$) have attracted much attention because of their ability to produce reactive species capable of reacting with organic matter in landfill leachate [10–13]. In general, the activation of PMS or PDS usually involves heterolytic or homolytic cleavage of the O-O bond to produce reactive oxygen species ($\text{SO}_4^{\bullet-}$ and HO^\bullet) [14–18]. For this reason, microwave (MW) heating is a widely used activation method in environmental water pollution treatment because of its unique penetration, rapidity, and other advantages [19–23].

However, compared with PDS, there have been few studies on the treatment of landfill leachate by the MW-activated PMS system (MW/PMS) [23]. This is because the

O-O bond dissociation energy of PDS ($E_{\text{PDS}} = +92$ kJ/mol) is lower than that of PMS ($E_{\text{PMS}} = +377$ kJ/mol) [24], which leads to facile conversion of PDS into $\text{SO}_4^{\bullet-}$ by thermal activation [25–28], whereas the one-electron transfer induced by metal reduction is more likely to activate PMS [29–33]. However, Ahn et al. found that the presence of Cl^- significantly improved the degradation of benzoic acid (BA) by heat-activated PMS under acidic conditions [34]. Landfill leachate contains not only a high concentration of refractory organic matter, but also a high concentration of Cl^- . However, the modification of the reactive species of the PMS oxidation system by Cl^- and its priority sequence for the removal of ammonia nitrogen and organic matter from landfill leachate remain unclear.

Theoretically, Cl^- can react with PMS, $\text{SO}_4^{\bullet-}$, and HO^\bullet to generate reactive chlorine species (RCS), such as monochloric radical (Cl^\bullet), dichloric radical ($\text{Cl}_2^{\bullet-}$), and hypochlorous acid (HOCl), which will greatly change the distribution of active species [35–40]. The polarity of the O-O bond in PMS makes it susceptible to attacks by Cl^- , which leads to nucleophilic addition reactions. PMS transfers an oxygen atom to Cl^- as a two-electron oxidant, resulting in HOCl as a secondary oxidant (Equation (1)) [41]. Through a series of reactions, Cl^- and HO^\bullet generate Cl^\bullet (Equations (2)–(4)), but $\text{SO}_4^{\bullet-}$ and Cl^- can directly generate Cl^\bullet through electron transfer (Equation (5)), and Cl^\bullet can continue to react to produce $\text{Cl}_2^{\bullet-}$ or even HOCl (Equations (6)–(9)) [29,36]. In contrast to a configured solution containing model pollutants, landfill leachate is real wastewater, in which the Cl^- concentration can reach thousands or even tens of thousands of milligrams per liter. The conversion in the PMS oxidation system is likely to be very complex, and its conversion law needs to be further studied.



In this study, the enhancing effect of Cl^- on the MW/PMS system has been investigated, with NH_4^+ -N as the main model pollutant; differences between conventional heating and the MW/PMS system with high Cl^- have been compared. Moreover, the conversion behavior of Cl^- in the MW/PMS system has been clarified by the quenching effects of alcohol reagents, the removal effect of NH_4^+ -N, and the chemical reactivity of characteristic organic matter. Finally, the priority sequence of removal of NH_4^+ -N and refractory organic matter from different types of landfill leachate has been revealed. It is hoped that this study will provide a theoretical basis for the design and optimization of MW/PMS systems to remove NH_4^+ -N and organic matter from landfill leachate with high Cl^- content.

2. Results and Discussion

2.1. Effects of Cl^- on NH_4^+ -N Removal by MW/PMS

To investigate the thermal and non-thermal effects of MW activation of PMS in a high-chloride ion background matrix [42], the removal of NH_4^+ -N by MW-activated PMS was compared with that by conventional water-bath-heated (heat)-activated PMS at the same activation temperature. As shown in Figure S1, the MW/PMS system showed a higher removal of NH_4^+ -N (93.50%) than the heat/PMS system (73.07%) at an NH_4^+ -N

concentration of 60 mg/L and a reaction temperature of 90 °C. It can be seen that the thermal effect of MW irradiation has a great influence on the activation of PMS under the conditions of a high-chloride ion background matrix, while the non-thermal effect can promote the activation of PMS to some extent.

The removal efficiencies of $\text{NH}_4^+\text{-N}$ by MW alone, PMS alone, and MW/PMS were compared in the presence and absence of Cl^- , with the aim of investigating the effect of Cl^- on the performance of MW/PMS. As shown in Figure 1a,b, in the absence of Cl^- , the $\text{NH}_4^+\text{-N}$ removal efficiencies with MW alone ($\text{pH}_0 = 3.0$), PMS alone, and MW/PMS were only 9.62%, 21.7%, and 23.48%, respectively. In the presence of Cl^- , there was no significant change in the removal efficiency of $\text{NH}_4^+\text{-N}$ by MW alone ($\text{pH}_0 = 3.0$). In the PMS-alone system, HOCl was formed directly by nucleophilic attack of Cl^- on PMS [41,43,44], which could then rapidly act on $\text{NH}_4^+\text{-N}$ to improve the removal efficiency. It is of interest that the removal of $\text{NH}_4^+\text{-N}$ in the MW/PMS system was significantly enhanced, especially at 17 mM Cl^- . Specifically, the removal efficiency was increased by 64.90%, and a further increase in the Cl^- concentration to 25.5 mM led to a further improvement in the removal efficiency of $\text{NH}_4^+\text{-N}$, as shown in Figure 1c,d, the removal rate increasing from 0.1805 to 0.3499 min^{-1} . In summary, increasing the Cl^- concentration effectively improved the removal of $\text{NH}_4^+\text{-N}$ by MW/PMS.

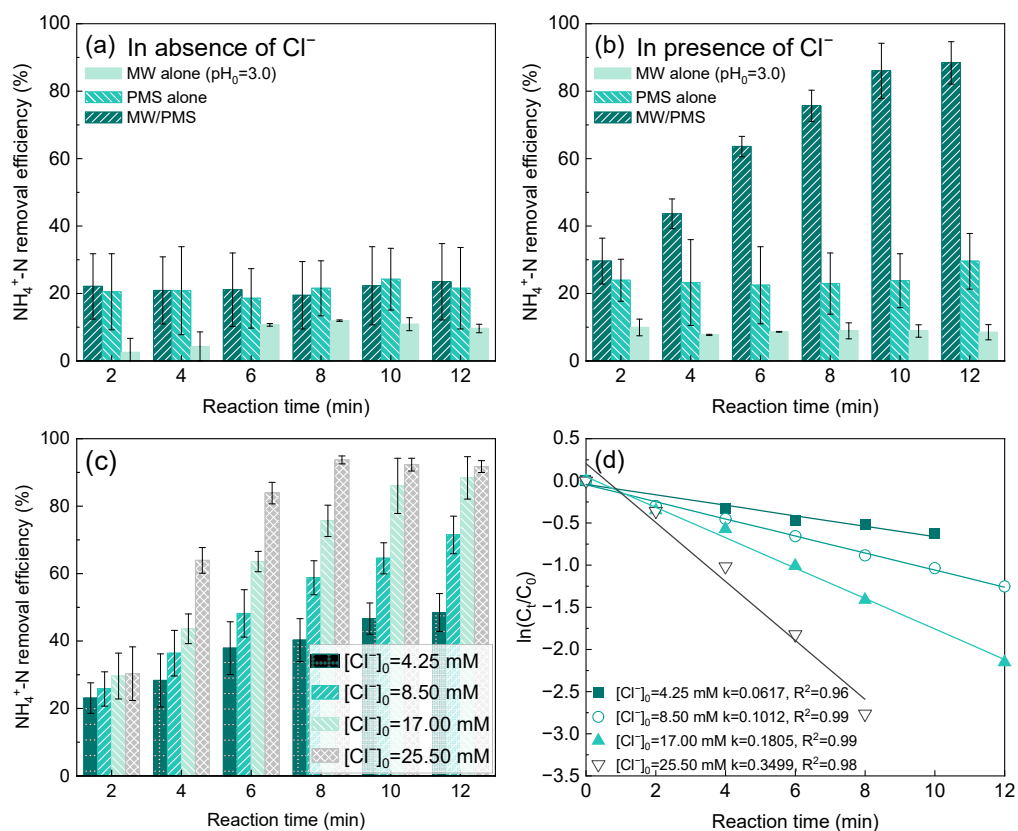


Figure 1. Effects of Cl^- on $\text{NH}_4^+\text{-N}$ removal. Removal of $\text{NH}_4^+\text{-N}$ by MW alone, PMS alone, and MW/PMS in (a) the presence and (b) absence of Cl^- , and the effects of Cl^- concentration on (c) $\text{NH}_4^+\text{-N}$ removal efficiency and (d) rate by the MW/PMS system. Reaction conditions: MW power = 160 W, $[\text{PMS}]_0 = 10$ mM, $[\text{Cl}^-]_0 = 17.00$ mM, and $[\text{NH}_4^+\text{-N}]_0 = 60$ mg/L.

2.2. Formation and Conversion of HOCl in a High- Cl^- Background Matrix

2.2.1. Formation Mechanism of HOCl

A high concentration of HOCl was found to be produced after the addition of Cl^- to the MW/PMS system (Figure 2a), reaching a maximum amount (753.73 μM) after a reaction time of 2 min. Thereafter, the amount of HOCl decreased with increasing reaction time. To

analyze the reason for the rapid production of HOCl in the early stage of the reaction (first 2 min) in a high-Cl⁻ background matrix, alcohol quenchers, namely *t*BuOH and EtOH, were added to the PMS alone and MW/PMS systems. *t*BuOH mainly acts as a quencher for HO• (*k**t*BuOH, HO• = 5.0 × 10⁸ M⁻¹ s⁻¹) and Cl• (*k**t*BuOH, Cl• = 6.2 × 10⁸ M⁻¹ s⁻¹), and EtOH is a quencher for HO• (*k*EtOH, HO• = 2.1 × 10⁹ M⁻¹ s⁻¹), SO₄^{•-} (*k*EtOH, SO₄^{•-} = 4.7 × 10⁷ M⁻¹ s⁻¹), and Cl• (*k*EtOH, Cl• = 1.7 × 10⁹ M⁻¹ s⁻¹) [34]. As shown in Figure 2a, the maximum cumulative concentration of HOCl was suppressed by the addition of *t*BuOH (by 46.75%) or EtOH (by 69.37%) to the MW/PMS system in the high-Cl⁻ background matrix at 2 min. Evidently, the ROS such as SO₄^{•-} and HO• generated in the MW/PMS system can react with Cl⁻ to generate HOCl.

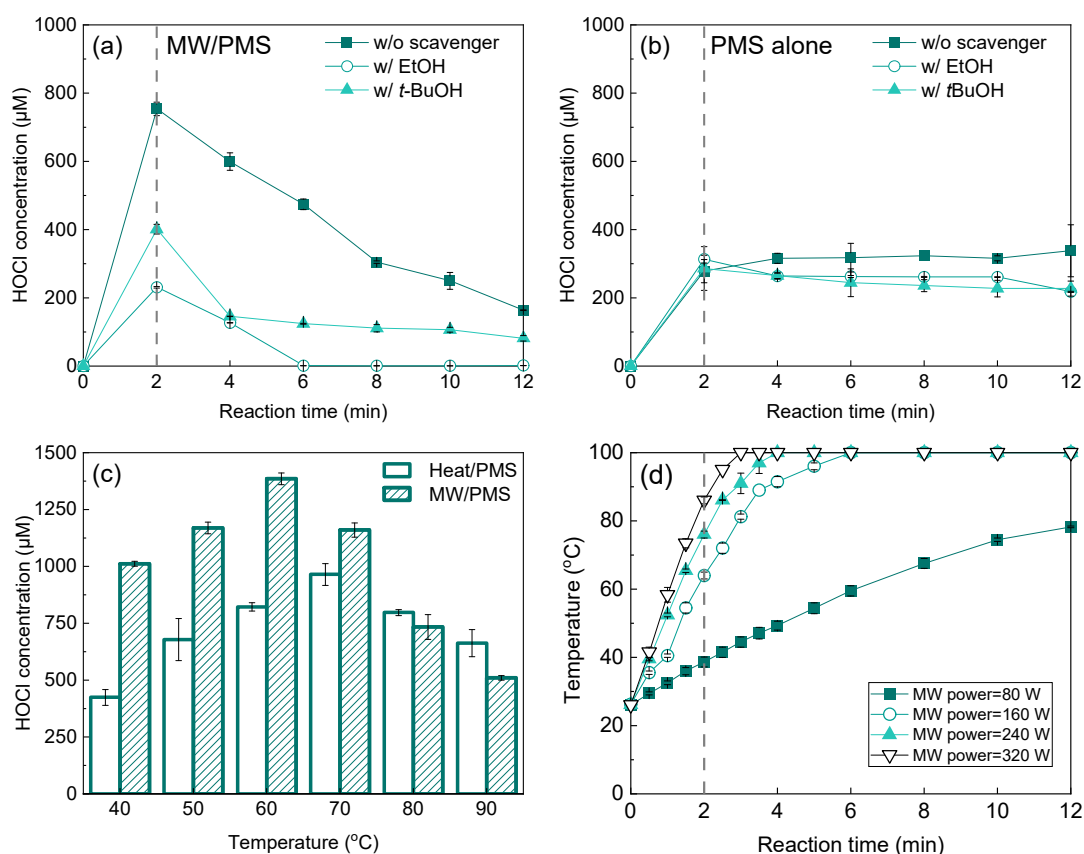


Figure 2. Effects of *t*BuOH and EtOH on the HOCl concentration in (a) MW/PMS and (b) PMS-alone systems in high-Cl⁻ background matrix, (c) comparison on the HOCl concentration of Heat/PMS and MW/PMS processes, and (d) effect of reaction temperature on HOCl concentration in MW/PMS and PMS-alone systems. Reaction conditions: MW power = 160 W, [PMS]₀ = 10 mM, [Cl⁻]₀ = 17.00 mM, [*t*BuOH]₀ = 100 mM, [EtOH]₀ = 100 mM, and reaction time = 8 min.

Wang et al. showed that PMS can generate HOCl directly by nucleophilic addition when the mass concentration ratio of Cl⁻ to oxidant is 1:1 [41,45]. To assess whether this idea holds in the present study, a PMS-alone system in a high-Cl⁻ background matrix was treated with 100 mM *t*BuOH and EtOH as molecular probes for SO₄^{•-} and HO•. Our results showed that the addition of *t*BuOH and EtOH had almost no effect on the HOCl concentration, indicating that PMS reacts directly with Cl⁻ to produce HOCl, consistent with previous studies [46].

Since the transfer of an oxygen atom from PMS to Cl⁻ is an endothermic reaction and an increase in temperature may favor the formation of a secondary oxidant (HOCl) [47], the effects of reaction temperature on the HOCl concentration in the MW/PMS and heat/PMS systems in a high-Cl⁻ background matrix were analyzed. In the heat/PMS system (Figure 2c), the HOCl concentration decreased after reaching a maximum (964.27 μM)

at 70 °C. In the MW/PMS system, a reaction temperature of 40–60 °C favored the production of HOCl, implying that PMS accelerates the oxidative conversion of Cl^- into HOCl under MW irradiation. However, the cumulative HOCl concentration gradually decreased from 1385.04 μM to 509.78 μM when the reaction temperature was further increased from 60 °C to 90 °C, indicating a noTable effect of temperature on the conversion of HOCl in the MW/PMS system. Combined with the temperature change curve of the system under MW irradiation (Figure 2d), it can be seen that the temperature of the system reached 60 °C after 2 min. In addition, it was observed that the presence of Cl^- increased the consumption of PMS (Figure S2). Therefore, the mechanism of the rapid formation of HOCl in the early stage of the reaction (2 min) is mainly due to (i) the formation of $\text{SO}_4^{\bullet-}$ and HO^\bullet by MW activating PMS, and (ii) the nucleophilic addition reaction of PMS with Cl^- .

2.2.2. Conversion of HOCl

The trends in the cumulative HOCl concentration in the MW/PMS system were compared at different Cl^- concentrations (Figure 3a,b). It was found that in the absence of $\text{NH}_4^+\text{-N}$, an increase in Cl^- concentration enhanced the maximum cumulative HOCl concentration in the early stage of the reaction. When $\text{NH}_4^+\text{-N}$ was present (60 mg/L), it caused a significant overall decrease in the cumulative HOCl concentration in the MW/PMS system. This result demonstrated that $\text{NH}_4^+\text{-N}$ can rapidly consume HOCl in this system.

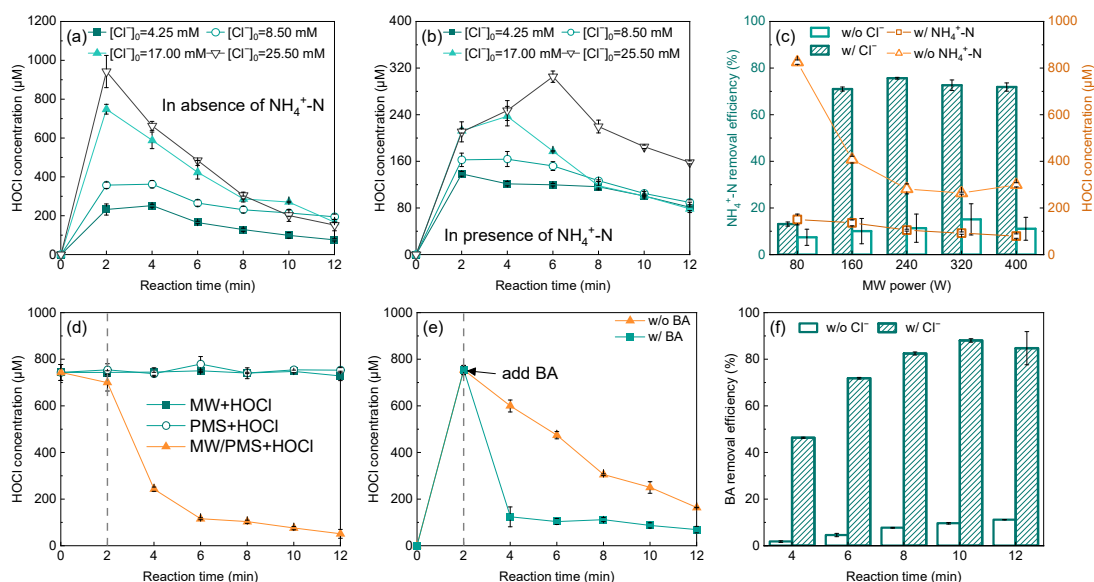


Figure 3. Effects of (a,b) Cl^- and (c) MW power on cumulative HOCl concentration in the MW/PMS system in absence and presence of $\text{NH}_4^+\text{-N}$. (d) Variation of HOCl concentration in MW-alone, PMS- alone, and MW/PMS systems when the HOCl initial concentration was $750.00 \pm 5 \mu\text{M}$ in the absence of $\text{NH}_4^+\text{-N}$. (e) Effects of benzoic acid (BA) on cumulative HOCl concentration in the MW/PMS system. (f) Effects of Cl^- on the BA removal efficiency in the MW/PMS system. Reaction conditions: MW power = 160 W, $[\text{PMS}]_0 = 10 \text{ mM}$, $[\text{Cl}^-]_0 = 17.00 \text{ mM}$, $[\text{HOCl}] = 750.00 \pm 5 \mu\text{M}$, $[\text{NH}_4^+\text{-N}]_0 = 60 \text{ mg/L}$, $[\text{BA}]_0 = 1 \text{ mM}$, and reaction time = 8 min.

To assess the role played by the generated HOCl in the system, the effect of MW power on the cumulative HOCl concentration of the MW/PMS system in a high- Cl^- background matrix was analyzed. As shown in Figure 3c, in the absence of $\text{NH}_4^+\text{-N}$, the cumulative HOCl concentration decreased with increasing MW power. In the presence of $\text{NH}_4^+\text{-N}$, the removal efficiency of this $\text{NH}_4^+\text{-N}$ gradually increased with increasing MW power, especially in the range 80–160 W. The amount of $\text{NH}_4^+\text{-N}$ removed increased from 7.85 mg/L to 42.60 mg/L, while the cumulative HOCl concentration decreased from 825.59 μM to 407.26 μM . As the MW power was increased, the change in the cumulative HOCl concentration apparently did not match the $\text{NH}_4^+\text{-N}$ removal. Moreover, in the absence of $\text{NH}_4^+\text{-N}$,

replacing Cl^- with HOCl to form the MW/HOCl system under otherwise constant reaction conditions (Figure 3d), the HOCl concentration was more stable with increasing reaction time. On this basis, the introduction of PMS in the MW/HOCl system, generating the MW/PMS/HOCl system, led to a very fast decay of the HOCl concentration. This implies that HOCl not only serves as an oxidant, but may also be involved in the removal of $\text{NH}_4^+\text{-N}$ as an activator of PMS.

Previous studies have shown that the $\text{SO}_4^{\bullet-}$ formed by HOCl-activated PMS can abstract an electron from Cl^- to form Cl^\bullet in a high- Cl^- content matrix and a high reaction temperature (60 °C) [34]. Therefore, it is conjectured that the decay of HOCl should be slower under conditions of PMS overload. Here, the effect of PMS concentration on HOCl decay was investigated under reaction conditions of an MW power of 160 W and a Cl^- concentration of 17.00 mM. When the PMS dosage was 1 mM in the absence of $\text{NH}_4^+\text{-N}$ (Figure S3a), there was no obvious decay trend of HOCl; however, when the PMS concentration was increased from 5 mM to 15 mM, the decay of HOCl in the MW/PMS system gradually increased, and its decay rate (Figure S3b) increased from 0.0912 to 0.1651 min^{-1} . It should be noted that when the PMS concentration was 15 mM in the presence of $\text{NH}_4^+\text{-N}$, the cumulative HOCl concentration showed an increasing trend after 6 min (Figure S4). This was presumably due to the progressive formation of reactive chlorine species such as Cl^\bullet , Cl_2^\bullet , and HOCl.

In the MW/PMS system, after 2 min of reaction, BA was introduced as a substrate. As shown in Figure 3e,f, the addition of Cl^- significantly accelerated the degradation of BA, and BA reduced the overall cumulative formation concentration of HOCl. BA is almost inert to HOCl but shows strong reactivity with Cl^\bullet ($k_{\text{BA}, \text{Cl}^\bullet} = 1.8 \times 10^{10} \text{ M}^{-1} \text{ s}^{-1}$) [48]. Therefore, the degradation of BA is independent of the production of HOCl in the Cl^- /MW/PMS system. The observations confirm that Cl^- can generate HOCl in the MW/PMS system, and that HOCl may be continuously transformed into Cl^\bullet .

Considering the influence of temperature on HOCl formation described in Section 2.2.1, it can be speculated that the transformation of Cl^- in the MW/PMS system involves the following pathways (Figure 4): (1) MW irradiation activates PMS to generate HO^\bullet and $\text{SO}_4^{\bullet-}$, which can react with Cl^- to generate Cl^\bullet , and Cl^\bullet can not only continue to react to generate HOCl but also participate in the degradation of organic matter as an oxidant; (2) the heating induced by MW irradiation promotes the nucleophilic addition of Cl^- to PMS, which can directly generate HOCl. On the one hand, in the presence of a sufficient amount of PMS, heat triggers the reaction between PMS and HOCl to form $\text{SO}_4^{\bullet-}$, which then reacts with Cl^- to form Cl^\bullet and HO^\bullet . On the other hand, HOCl can react with $\text{SO}_4^{\bullet-}$ to form chlorate (ClO_3^-) [49,50], but not in large quantities.

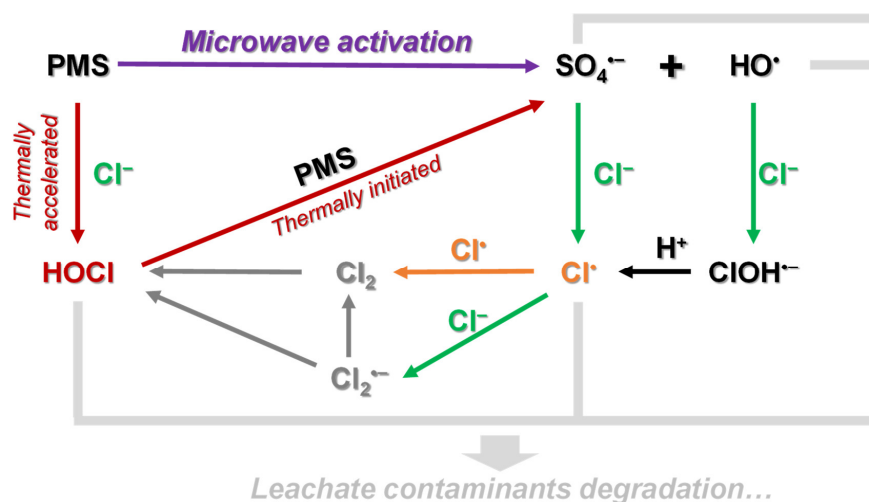


Figure 4. Proposed transformation pathways of Cl^- in the MW/PMS system.

2.3. Influence of the Background Matrix

In addition to Cl^- , HA and inorganic anions such as CO_3^{2-} , HCO_3^- , and NO_3^- are also present in landfill leachate. These substances may have a certain influence on the removal of ammonia nitrogen by the MW/PMS system under the background of high Cl^- content.

Figure 5a,b clearly shows that the addition of CO_3^{2-} , HCO_3^- , NO_3^- , and HA inhibits the removal of ammonia nitrogen, and the order of inhibition abilities is $\text{CO}_3^{2-} < \text{HCO}_3^- < \text{NO}_3^- < \text{HA}$. It is speculated that CO_3^{2-} , HCO_3^- , NO_3^- , and HA can compete with ammonia nitrogen for active species ($\text{SO}_4^{\bullet-}$, Cl^{\bullet} , and HOCl) in the MW/PMS system. Among them, CO_3^{2-} , HCO_3^- , and NO_3^- can react with $\text{SO}_4^{\bullet-}$ to generate $\text{CO}_3^{\bullet-}$, HCO_3^{\bullet} , and NO_3^{\bullet} , respectively [45,51]. Moreover, CO_3^{2-} may be partially hydrolyzed to HCO_3^- in aqueous solution, resulting in the consumption of active species in the system and a reduction of the ammonia nitrogen removal efficiency. Meanwhile, HA, as one of the main components of natural organic matter (NOM), is a non-uniform macromolecular polymer. Its molecular structure is complex and contains many organic functional groups, such as hydroxyl, carboxyl, carbonyl, methoxy, and quinone groups [52]. It can compete with ammonia nitrogen for active species, thus reducing the removal efficiency of ammonia nitrogen by the MW/PMS system.

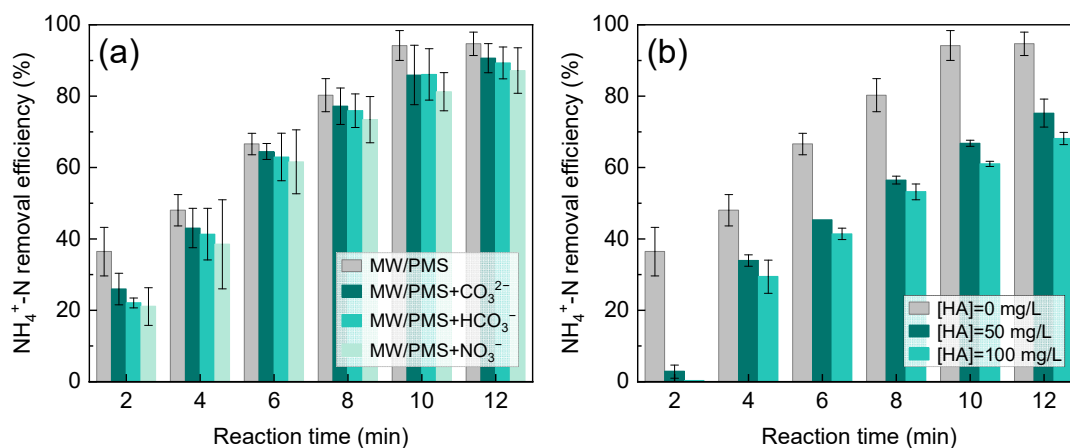


Figure 5. Effects of inorganic anions (a) and humus (b) on ammonia nitrogen removal in the MW/PMS system under a high- Cl^- background. Reaction conditions: MW power = 160 W, $[\text{PMS}]_0 = 10$ mM, $[\text{Cl}^-]_0 = 17.00$ mM, $[\text{NH}_4^+-\text{N}]_0 = 60$ mg/L, $[\text{inorganic anion}] = 100$ mg/L, $[\text{HA}] = 50, 100$ mg/L.

2.4. Effect of Ammonia Nitrogen on the Removal of Organic Matter from High-Chloride Landfill Leachate by the MW/PMS System

To further clarify the effect on reactivity of high concentrations of Cl^- in the simultaneous presence of ammonia nitrogen and organic matter in the MW/PMS system, its effects on the accumulation and generation of HOCl , transformation of ammonia nitrogen, and removal of TOC were evaluated by varying the ammonia nitrogen concentration in ML and ROCL. Moreover, 3D-EEM was used to analyze the transformation characteristics of refractory organic matter (humus).

2.4.1. Influence of Ammonia Nitrogen on the Organic Matter Removal Effect

As shown in Figure 6a–f, under the same reaction conditions (MW power = 160 W, $[\text{PMS}]_0 = 10$ mM), increasing ammonia nitrogen concentration led to suppression of the maximum cumulative concentration of HOCl and the removal efficiencies of ammonia nitrogen and TOC from ML and ROCL effluents, but the degrees of inhibition were different. Taking an increase in ammonia nitrogen concentration from 0 to 60 mg/L as an example, under the same reaction conditions (MW power = 160 W, $[\text{PMS}]_0 = 10$ mM), the maximum cumulative concentration of HOCl in ML effluent decreased from 222.28 μM (4 min) to

174.03 μM (4 min), and the removal efficiencies of ammonia nitrogen and TOC (12 min) decreased from 100% to 51.06% and from 40.47% to 18.96%, respectively. Likewise, the maximum cumulative concentration of HOCl in ROCL effluent decreased significantly from 1693.29 μM (4 min) to 398.12 μM (6 min), and the removal efficiencies of ammonia nitrogen and TOC (12 min) decreased from 100% to 70.53% and from 78.45% to 72.62%, respectively. On the one hand, there is relatively little organic matter in ROCL ($\text{TOC}_{\text{ROCL}} = 10.03 \text{ mg/L}$). Under these experimental conditions, the organics in ROCL are preferentially mineralized by the MW/PMS system. At this stage, there are still enough active species in the system that can continue to react with ammonia nitrogen, so the increase in ammonia nitrogen concentration has little effect on the removal of organics from ROCL. On the other hand, due to the relatively large amount of organics in ML ($\text{TOC}_{\text{ML}} = 118.70 \text{ mg/L}$), it cannot be completely mineralized by the MW/PMS system. Since some organic matter still exists in the system, there is a competition between ammonia nitrogen and organic matter for active species in the MW/PMS system, thus reducing the treatment performance.

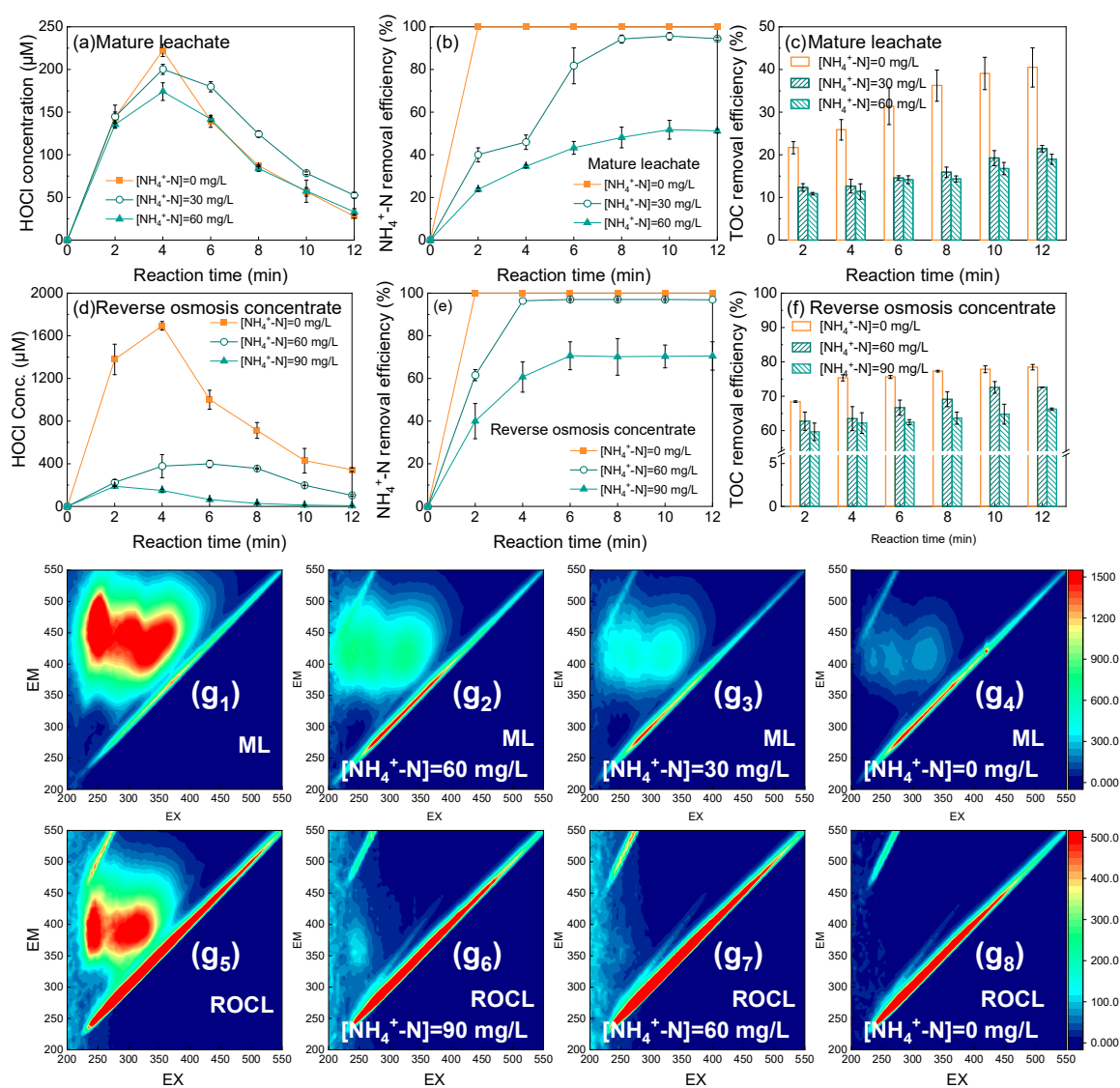


Figure 6. Cumulative concentration of HOCl and removal efficiencies of ammonia nitrogen and TOC in aged landfill leachate (a–c) and reverse osmosis concentrate (d–f) treated by the MW/PMS system under different conditions of ammonia nitrogen. Comparison of the three-dimensional fluorescence spectra (g) before and after reaction. Reaction conditions: MW power = 160 W, $[\text{PMS}]_0 = 10 \text{ mM}$, $[\text{Cl}^-]_{\text{ML}} = 20.34 \text{ mM}$, $[\text{Cl}^-]_{\text{ROCL}} = 44.26 \text{ mM}$, reaction time=12 min.

2.4.2. 3D-EEM Analysis

The refractory organics in landfill leachate are mainly humus, including HA and FA, which have strong fluorescence absorption characteristics. Generally, the larger the conjugated system, the stronger the fluorescence intensity [1,53–55]. According to previous studies, fulvic acid A (Ex 200–275 nm, Em 380–550 nm), HA C (Ex 275–400 nm, Em 380–550 nm), low-excitation tryptophan S (Ex 200–250 nm, Em 330–380 nm), high-excitation tryptophan T (Ex 250–300 nm, Em 330–380 nm), low-excitation tyrosine D (Ex 200–250 nm, Em 280–330 nm), and high-excitation tyrosine B (Ex 250–300 nm, Em 280–330 nm) can be analyzed by 3D-EEM [56].

As shown in Figure 6g₁,g₅, the 3D-EEM spectra of ROCL and ML have strong fluorescence intensity in the region in which FA and HA are located. According to Table S1, both ML and ROCL evidence the kurtosis of conjugated double bonds and benzene ring structures and have a high degree of condensation, which indicates that the organics therein are difficult to degrade.

After ROCL and ML were each treated by the MW/PMS system (Figure 6g₄,g₈), the fluorescence intensities in the regions corresponding to FA and HA in the spectra of the effluents decreased significantly, the peak positions of the fluorescence were distinctly blue-shifted, and the peaks of FA and HA were decreased to varying degrees. This shows that the MW/PMS system can effectively reduce the humification degree of refractory organic matter in high-chloride landfill leachate. On this basis, with the increase in ammonia nitrogen concentration, the condensation degree and fluorescence peak intensities of FA and HA in ML (Figure 6g₂,g₃) and ROCL (Figure 6g₆,g₇) increased to some extent; that is, the higher the initial ammonia nitrogen concentration in landfill leachate, the lower the humus removal efficiency. From Figure S5, it is clear that the presence of ammonia nitrogen increases the maximum peak intensity ratio of FA organics after treatment by the MW/PMS system, especially in ROCL, which shows that when ammonia nitrogen co-exists with organics, HA will be preferentially removed by the MW/PMS system, resulting in the retention of FA organics. A high concentration of ammonia nitrogen can inhibit the degradation of humus in landfill leachate by the MW/PMS system to a certain extent, especially the removal efficiency of FA organics.

3. Materials and Methods

3.1. Experimental Water Sample and Reagents

Mature landfill leachate (ML) and reverse osmosis concentrated leachate (ROCL) were collected from a large anaerobic landfill in southwest China, which was built in 1992 and has a total storage capacity of 32.09 million m³. The intrinsic color of ML was dark-brown, and its total organic carbon (TOC) concentration, NH₄⁺-N, and Cl⁻ contents were 11,870, 300.90, and 11,829.8 mg/L, respectively. The color of the ROCL was pale-yellow, and its TOC, NH₄⁺-N, and Cl⁻ contents were 100.25, 4.74, and 15,689.90, respectively. The landfill leachate was sealed in a vessel and stored at 4 °C in the dark prior to subsequent experiments.

Potassium monoperoxysulfate (PMS, KHSO₅·0.5KHSO₄·0.5K₂SO₄) was provided by Merck Reagents. Sodium chloride (NaCl), aqueous ammonia (NH₄OH), benzoic acid (C₇H₆O₂) (BA), sodium hydrogencarbonate (NaHCO₃), sodium carbonate (Na₂CO₃), sodium nitrate ((NaNO₃), concentrated sulfuric acid (H₂SO₄), sodium hydroxide (NaOH), Nessler reagent (K₂HgI₄), potassium sodium tartrate (C₄H₄KNaO₆), *N,N*-diethyl-*p*-phenyl enediamine sulfate (C₁₀H₁₆N₂·H₂SO₄; DPD), disodium ethylenediamine-tetraacetate ([-CH₂N(CH₂CO₂Na)CH₂CO₂H]₂; EDTA), disodium hydrogenphosphate (Na₂HPO₄), and potassium dihydrogenphosphate (KH₂PO₄) were provided by Chron Chemical (Chengdu, China). All reagents used in the experiments were of analytical grade. The water used in the experiments was secondary reverse osmosis ultra-pure water (18.2 MΩ-cm) produced by a UIPZYDRO-200 apparatus (Youpu Equipment Co. Ltd., Chengdu, China).

3.2. Experimental Procedure

Aqueous test medium (100 mL) was accurately measured with a measuring cylinder and transferred to a 250 mL brown round-bottomed flask, and predetermined amounts of NaCl, NH₄OH, and oxidizing agent (PMS) were successively added. Without adjusting the pH, the solution was immediately placed in a professional microwave chemical reactor (MCR-3, Yuhua Instrument Co., Ltd., Gongyi, China), and the reaction was timed. The reflux condensation device was turned on during the reaction to reduce the evaporation of water. After the reaction, the solution was immediately placed in an ice-water bath and cooled to room temperature (5 min) in the dark. It was rapidly filtered through a 0.45 μM filter membrane, and the HOCl and NH₄⁺-N contents and pH of the filtrate were analyzed.

Experiments with landfill leachate were carried out in the same way. The treated landfill leachate effluent was collected at a predetermined time and divided into two parts. One part was determined immediately for HOCl, NH₄⁺-N, and TOC. The other portion of the mixture was quenched with ethanol for 3D-excitation and emission matrix (EEM) analysis. The ML selected for this study contained a large amount of humus and other refractory organic matter, and its intrinsic color (dark-brown) interfered with the determination of HOCl in the MW/PMS system. Therefore, it was diluted 100-fold with secondary reverse osmosis ultra-pure water. However, the Cl⁻ concentration in the ML after dilution was only 3.34 mM. To better study the HOCl generated in the ML under the experimental conditions (MW = 160 W, [PMS] = 10 mM), an additional 17 mM Cl⁻ was added to the test medium ([Cl⁻]_{ML} = 20.34 mM, [NH₄⁺-N]_{ML} ≈ 0 mM, [TOC]_{ML} = 118.70 mg/L). The ROCL, which contained a large amount of Cl⁻ (442.59 mM), was diluted 10-fold, like the test medium, so as to compare the production of HOCl in the ML under the experimental conditions and to regulate the concentration of ammonia nitrogen ([Cl⁻]_{ROCL} = 44.26 mM, [NH₄⁺-N]_{ROCL} ≈ 0 mM, [TOC]_{ROCL} = 10.03 mg/L). All experiments were performed in duplicate.

3.3. Analysis Methods

The pH of the water samples was determined by a multiparameter water quality analyzer (DZS-708-A, INESA Scientific Instrument Co., Ltd., Shanghai, China). TOC was determined by a total organic carbon/total nitrogen analyzer (Multi N/C 3100, Analytik GmbH, Jena, Germany). The concentrations of HOCl and NH₄⁺-N were determined by means of an ultraviolet/visible/near-infrared (UV/Vis/NIR) spectrophotometer (Lambda 950, Perkin-Elmer, USA). The HOCl concentration was determined by spectrophotometric determination of its complex with DPD, and the NH₄⁺-N concentration was determined by spectrophotometric determination of its complex with Nessler reagent. The standard curve is shown in Figure S6.

Three-dimensional excitation and emission matrix (3D-EEM) spectra (F-7000, Hitachi, Japan) were used to determine fluorescent dissolved organic matter (DOM) in landfill leachate water samples. The fixed excitation and emission wavelengths were in the range 200–550 nm. The scanning interval was 5 nm and the scanning rate was 2400 nm/min.

4. Conclusions

This study investigated the modification of reactive species of the PMS oxidation system by Cl⁻ and its priority sequence for the removal of NH₄⁺-N and organic matter from landfill leachate. The results showed that under acidic conditions, increasing the Cl⁻ concentration can effectively improve the ammonia nitrogen removal efficiency of the MW/PMS system and generate a certain amount of HOCl. Moreover, the thermal and non-thermal effects of MW have a significant influence on the activation of PMS to form HOCl. The formation pathways of HOCl include (i) the reactions of SO₄^{•-} and HO[•] formed by MW activation of PMS with Cl⁻ and (ii) the nucleophilic addition reaction of PMS and Cl⁻. Furthermore, the high concentration of HOCl produced by the system can also react with PMS to continuously generate Cl[•] as an oxidant to participate in the reaction with pollutants (ammonia nitrogen and organic matter). Finally, the removal behavior

of ammonia nitrogen and DOM co-existing in actual high-chloride landfill leachate was investigated. It was found that ammonia nitrogen and DOM would compete for active species, HA would be preferentially removed, and fulvic acid would remain.

Supplementary Materials: The following supporting information can be downloaded at: <https://www.mdpi.com/article/10.3390/catal12101078/s1>, Figure S1: The NH_4^+ -N removal efficiency and effluent pH of MW/PMS and Heat/PMS systems under high Cl^- concentration. Reaction conditions: MW power = 160 W, $[\text{PMS}]_0 = 10 \text{ mM}$, $[\text{Cl}^-]_0 = 17.00 \text{ mM}$, and $[\text{NH}_4^+\text{-N}]_0 = 60 \text{ mg/L}$, and reaction time = 8 min; Figure S2: Effects of Cl^- on PMS concentration. Reaction conditions: MW power = 160 W, $[\text{PMS}]_0 = 10 \text{ mM}$, and $[\text{Cl}^-]_0 = 17.00 \text{ mM}$; Figure S3: Effects of PMS concentration on (a) cumulative HOCl concentration and (b) HOCl decay in MW/PMS system. Reaction conditions: MW power = 160 W and $[\text{Cl}^-]_0 = 17.00 \text{ mM}$; Figure S4: Effects of PMS concentration on cumulative HOCl concentration in presence of NH_4^+ -N in the MW/PMS system. Reaction conditions: MW power = 160 W, $[\text{Cl}^-]_0 = 17.00 \text{ mM}$, and $[\text{NH}_4^+\text{-N}]_0 = 60 \text{ mg/L}$; Figure S5: Proportion of humic- (HA) and fulvic-like matter (FA). Reaction time: MW power = 160 W, $[\text{Cl}^-]_{\text{ML}} = 20.34 \text{ mM}$, $[\text{Cl}^-]_{\text{ROCL}} = 44.26 \text{ mM}$, $[\text{NH}_4^+\text{-N}]_0 = 60 \text{ mg/L}$, and reaction time = 12 min; Figure S6: Standard curves of (a) HOCl concentration against absorbance and (b) NH_4^+ -N concentration against absorbance; Table S1: Fluorescence peak position and intensity for ML and ROCL subjected to MW/PMS treatment at NH_4^+ concentration.

Author Contributions: K.F.: Conceptualization, methodology, validation, formal analysis, investigation, writing—original draft preparation, writing—review and editing, visualization; Q.L.: Conceptualization, methodology, writing—review and editing, supervision, project administration, funding acquisition. All authors have read and agreed to the published version of the manuscript.

Funding: This research was funded by the Chengdu Science and Technology Bureau (2021-YF05-00057-SN).

Data Availability Statement: Not applicable.

Acknowledgments: This study was supported by Chengdu Science and Technology Bureau (2021-YF05-00057-SN).

Conflicts of Interest: There are no conflict of interest to declare.

References

1. Chen, W.; Zhuo, X.; He, C.; Shi, Q.; Li, Q. Molecular investigation into the transformation of dissolved organic matter in mature landfill leachate during treatment in a combined membrane bioreactor-reverse osmosis process. *J. Hazard. Mater.* **2020**, *397*, 122759. [[CrossRef](#)] [[PubMed](#)]
2. Cheng, H.; Hu, Y. Municipal solid waste (MSW) as a renewable source of energy: Current and future practices in China. *Bioresour. Technol.* **2010**, *101*, 3816–3824. [[CrossRef](#)] [[PubMed](#)]
3. Gu, Z.; Chen, W.; Li, Q.; Zhang, A. Treatment of semi-aerobic aged-refuse biofilter effluent from treating landfill leachate with the Fenton method. *Process Saf. Environ. Prot.* **2020**, *133*, 32–40. [[CrossRef](#)]
4. Wu, C.; Chen, W.; Gu, Z.; Li, Q. A review of the characteristics of Fenton and ozonation systems in landfill leachate treatment. *Sci. Total Environ.* **2021**, *762*, 143131. [[CrossRef](#)]
5. Yan, Z.; Lu, Z.; Chen, X.; Jiang, Y.; Huang, Z.; Liu, L.; Fan, G.; Chang, H.; Qu, F.; Liang, H. Membrane distillation treatment of landfill leachate: Characteristics and mechanism of membrane fouling. *Sep. Purif. Technol.* **2022**, *289*, 120787. [[CrossRef](#)]
6. Zhang, J.; Xiao, K.; Huang, X. Full-scale MBR applications for leachate treatment in China: Practical, technical, and economic features. *J. Hazard. Mater.* **2020**, *389*, 122138. [[CrossRef](#)]
7. Gu, Z.; Chen, W.; He, C.; Li, Q. Molecular insights into the transformation of refractory organic matter in landfill leachate nanofiltration concentrates during a flocculation and $\text{O}_3/\text{H}_2\text{O}_2$ treatment. *J. Hazard. Mater.* **2022**, *435*, 128973. [[CrossRef](#)]
8. Chen, W.; Gu, Z.; Ran, G.; Li, Q. Application of membrane separation technology in the treatment of leachate in China: A review. *Waste Manag.* **2021**, *121*, 127–140. [[CrossRef](#)]
9. Gu, Z.; Feng, K.; Li, Y.; Li, Q. Microbial characteristics of the leachate contaminated soil of an informal landfill site. *Chemosphere* **2022**, *287*, 132155. [[CrossRef](#)]
10. Chen, C.; Feng, H.; Deng, Y. Re-evaluation of sulfate radical based-advanced oxidation processes (SR-AOPs) for treatment of raw municipal landfill leachate. *Water Res.* **2019**, *153*, 100–107. [[CrossRef](#)]
11. Chen, S.; He, Z. Sono-electrochemical activation of peroxymonosulfate: Influencing factors and mechanism of FA degradation, and application on landfill leachate treatment. *Chemosphere* **2021**, *296*, 133365. [[CrossRef](#)]

12. Chen, M.; He, Y.; Gu, Z. Microwave irradiation activated persulfate and hydrogen peroxide for the treatment of mature landfill leachate effluent from a membrane bioreactor. *Sep. Purif. Technol.* **2020**, *250*, 117111. [[CrossRef](#)]
13. Pan, X.; Gu, Z.; Chen, W.; Li, Q. Preparation of biochar and biochar composites and their application in a Fenton-like process for wastewater decontamination: A review. *Sci. Total Environ.* **2021**, *754*, 142104. [[CrossRef](#)]
14. Amanollahi, H.; Moussavi, G.; Giannakis, S. Enhanced vacuum UV-based process (VUV/H₂O₂/PMS) for the effective removal of ammonia from water: Engineering configuration and mechanistic considerations. *J. Hazard. Mater.* **2021**, *402*, 123789. [[CrossRef](#)]
15. Anipsitakis, G.P.; Dionysiou, D.D.; Gonzalez, M.A. Cobalt-Mediated Activation of Peroxymonosulfate and Sulfate Radical Attack on Phenolic Compounds. Implications of Chloride Ions. *Environ. Sci. Technol.* **2006**, *40*, 1000–1007. [[CrossRef](#)]
16. Anipsitakis, G.P.; Dionysios, D.D. Degradation of Organic Contaminants in Water with Sulfate Radicals Generated by the Conjunction of Peroxymonosulfate with Cobalt. *Environ. Sci. Technol.* **2003**, *37*, 4749–4797. [[CrossRef](#)]
17. Chan, K.H.; Chu, W. Degradation of atrazine by cobalt-mediated activation of peroxymonosulfate: Different cobalt counteranions in homogenous process and cobalt oxide catalysts in photolytic heterogeneous process. *Water Res.* **2009**, *43*, 2513–2521. [[CrossRef](#)]
18. Lee, J.; von Gunten, U.; Kim, J.H. Persulfate-Based Advanced Oxidation: Critical Assessment of Opportunities and Roadblocks. *Environ. Sci. Technol.* **2020**, *54*, 3064–3081. [[CrossRef](#)]
19. Chen, W.; Wang, F.; He, C.; Li, Q. Molecular-level comparison study on microwave irradiation-activated persulfate and hydrogen peroxide processes for the treatment of refractory organics in mature landfill leachate. *J. Hazard. Mater.* **2020**, *397*, 122785. [[CrossRef](#)]
20. Xia, H.; Li, C.; Yang, G.; Shi, Z.; Jin, C.; He, W.; Xu, J.; Li, G. A review of microwave-assisted advanced oxidation processes for wastewater treatment. *Chemosphere* **2022**, *287*, 131981. [[CrossRef](#)]
21. Dai, Y.; Qi, C.; Cao, H.; Wen, Y.; Zhao, Y.; Xu, C.; Yang, S.; He, H. Enhanced degradation of sulfamethoxazole by microwave-activated peracetic acid under alkaline condition: Influencing factors and mechanism. *Sep. Purif. Technol.* **2022**, *288*, 120716. [[CrossRef](#)]
22. Qi, C.; Chen, H.; Xu, C.; Xu, Z.; Chen, H.; Yang, S.; Li, S.; He, H.; Sun, C. Synthesis and application of magnetic materials-barium ferrite nanomaterial as an effective microwave catalyst for degradation of brilliant green. *Chemosphere* **2020**, *260*, 127681. [[CrossRef](#)]
23. Qi, C.; Liu, X.; Lin, C.; Zhang, H.; Li, X.; Ma, J. Activation of peroxymonosulfate by microwave irradiation for degradation of organic contaminants. *Chem. Eng. J.* **2017**, *315*, 201–209. [[CrossRef](#)]
24. Benson, S.W. Thermochemistry and Kinetics of Sulfur-Containing Molecules and Radicals. *Chemical Reviews* **1978**, *78*, 23–35. [[CrossRef](#)]
25. Chen, W.; Gu, Z.; Guo, S.; Li, Q. Microwave-assisted Fe⁰-activated persulfate process for treating explosives in production wastewater. *Chem. Eng. J.* **2020**, *391*, 123497. [[CrossRef](#)]
26. Chen, W.; Luo, Y.; Ran, G.; Li, Q. An investigation of refractory organics in membrane bioreactor effluent following the treatment of landfill leachate by the O₃/H₂O₂ and MW/PS processes. *Waste Manag.* **2019**, *97*, 1–9. [[CrossRef](#)]
27. Chen, W.; Luo, Z.; Wu, C.; Wen, P.; Li, Q. Oxidative removal of recalcitrant organics in shale gas flowback fluid by the microwave-activated persulfate process. *Environ. Sci. Pollut. Res.* **2019**, *26*, 684–693. [[CrossRef](#)]
28. Yang, P.; Ji, Y.; Lu, J.; Huang, Q. Formation of Nitrophenolic Byproducts during Heat-Activated Peroxydisulfate Oxidation in the Presence of Natural Organic Matter and Nitrite. *Environ. Sci. Technol.* **2019**, *53*, 4255–4264. [[CrossRef](#)]
29. Chen, T.; Yu, Z.; Xu, T.; Xiao, R.; Chu, W.; Yin, D. Formation and degradation mechanisms of CX3R-type oxidation by-products during cobalt catalyzed peroxymonosulfate oxidation: The roles of Co³⁺ and SO₄^{•-}. *J. Hazard. Mater.* **2021**, *405*, 124243. [[CrossRef](#)]
30. Wang, S.; Wang, J. Synergistic effect of PMS activation by Fe⁰@Fe₃O₄ anchored on N, S, O co-doped carbon composite for degradation of sulfamethoxazole. *Chem. Eng. J.* **2022**, *427*, 131960. [[CrossRef](#)]
31. Wang, S.; Hu, J.; Wang, J. Degradation of sulfamethoxazole using PMS activated by cobalt sulfides encapsulated in nitrogen and sulfur co-doped graphene. *Sci. Total Environ.* **2022**, *827*, 154379. [[CrossRef](#)] [[PubMed](#)]
32. Wang, J.; B, H.; Yang, M.; Liu, R.; Hu, C.; Liu, H.; Qu, J. Anaerobically-digested sludge disintegration by transition metal ions-activated peroxymonosulfate (PMS): Comparison between Co²⁺, Cu²⁺, Fe²⁺ and Mn²⁺. *Sci. Total Environ.* **2020**, *713*, 136530. [[CrossRef](#)] [[PubMed](#)]
33. Qi, C.; Liu, X.; Lin, C.; Zhang, X.; Ma, J.; Tan, H.; Ye, W. Degradation of sulfamethoxazole by microwave-activated persulfate: Kinetics, mechanism and acute toxicity. *Chem. Eng. J.* **2014**, *249*, 6–14. [[CrossRef](#)]
34. Ahn, Y.Y.; Choi, J.; Kim, M.; Kim, M.S.; Lee, D.; Bang, W.H.; Yun, E.T.; Lee, H.; Lee, J.H.; Lee, C.; et al. Chloride-Mediated Enhancement in Heat-Induced Activation of Peroxymonosulfate: New Reaction Pathways for Oxidizing Radical Production. *Environ. Sci. Technol.* **2021**, *55*, 5382–5392. [[CrossRef](#)]
35. Yu, X.; Bao, Z.; Barker, J.R. Free Radical Reactions Involving Cl[•], Cl₂^{•-}, and SO₄^{•-} in the 248 nm Photolysis of Aqueous Solutions Containing S₂O₈²⁻ and Cl⁻. *J. Phys. Chem. A* **2004**, *102*, 295–308. [[CrossRef](#)]
36. Yuan, R.; Ramjaun, S.N.; Wang, Z.; Liu, J. Effects of chloride ion on degradation of Acid Orange 7 by sulfate radical-based advanced oxidation process: Implications for formation of chlorinated aromatic compounds. *J. Hazard. Mater.* **2011**, *196*, 173–179. [[CrossRef](#)]
37. Zheng, Y.; Xie, H.; Sun, B.; Zhang, J.; Wang, W. The altered effects of chloride on the treatment efficiency of SO₄⁻-based AOPs by other background water constituents. *Chem. Eng. J.* **2022**, *441*, 135914. [[CrossRef](#)]

38. Li, C.-X.; Chen, C.-B.; Wang, Y.-J.; Fu, X.-Z.; Cui, S.; Lu, J.-Y.; Li, J.; Liu, H.-Q.; Li, W.-W.; Lau, T.-C. Insights on the pH-dependent roles of peroxymonosulfate and chlorine ions in phenol oxidative transformation. *Chem. Eng. J.* **2019**, *362*, 570–575. [[CrossRef](#)]
39. Lu, Q.; Liu, Y.; Li, B.; Feng, L.; Du, Z.; Zhang, L. Reaction kinetics of dissolved black carbon with hydroxyl radical, sulfate radical and reactive chlorine radicals. *Sci. Total Environ.* **2022**, *828*, 153984. [[CrossRef](#)]
40. Peng, J.; Wang, Z.; Wang, S.; Liu, J.; Zhang, Y.; Wang, B.; Gong, Z.; Wang, M.; Dong, H.; Shi, J.; et al. Enhanced removal of methylparaben mediated by cobalt/carbon nanotubes (Co/CNTs) activated peroxymonosulfate in chloride-containing water: Reaction kinetics, mechanisms and pathways. *Chem. Eng. J.* **2021**, *409*, 128176. [[CrossRef](#)]
41. Wang, S.; Wang, J. Treatment of membrane filtration concentrate of coking wastewater using PMS/chloridion oxidation process. *Chem. Eng. J.* **2020**, *379*, 122361. [[CrossRef](#)]
42. Bose, S.; Kumar, M. Microwave-assisted persulfate/peroxymonosulfate process for environmental remediation. *Curr. Opin. Chem. Eng.* **2022**, *36*, 100826. [[CrossRef](#)]
43. Patton, S.D.; Dodd, M.C.; Liu, H. Degradation of 1,4-dioxane by reactive species generated during breakpoint chlorination: Proposed mechanisms and implications for water treatment and reuse. *J. Hazard. Mater. Lett.* **2022**, *3*, 100054. [[CrossRef](#)]
44. Zhang, Y.; Li, J.; Bai, J.; Li, L.; Chen, S.; Zhou, T.; Wang, J.; Xia, L.; Xu, Q.; Zhou, B. Extremely Efficient Decomposition of Ammonia N to N₂ Using ClO(*) from Reactions of HO(*) and HOCl Generated in Situ on a Novel Bifacial Photoelectroanode. *Environ. Sci. Technol.* **2019**, *53*, 6945–6953. [[CrossRef](#)]
45. Wang, J.; Wang, S. Effect of inorganic anions on the performance of advanced oxidation processes for degradation of organic contaminants. *Chem. Eng. J.* **2021**, *411*, 128392. [[CrossRef](#)]
46. Zeng, H.; Zhao, X.; Zhao, F.; Park, Y.; Repo, E.; Thangaraj, S.K.; Janis, J.; Sillanpaa, M. Oxidation of 2,4-dichlorophenol in saline water by unactivated peroxymonosulfate: Mechanism, kinetics and implication for in situ chemical oxidation. *Sci. Total Environ.* **2020**, *728*, 138826. [[CrossRef](#)]
47. Lente, G.; Kalmár, J.; Baranyai, Z.; Kun, A.; Kék, I.; Bajusz, D.; Takács, M.; Veres, L.; Fábián, I. One- Versus Two-Electron Oxidation with Peroxomonosulfate Ion: Reactions with Iron(II), Vanadium(IV), Halide Ions, and Photoreaction with Cerium(III). *Inorg. Chem.* **2009**, *48*, 1763–1773. [[CrossRef](#)]
48. Deborde, M.; von Gunten, U. Reactions of chlorine with inorganic and organic compounds during water treatment-Kinetics and mechanisms: A critical review. *Water Res.* **2008**, *42*, 13–51. [[CrossRef](#)]
49. Li, Z.; Chen, Z.; Xiang, Y.; Ling, L.; Fang, J.; Shang, C.; Dionysiou, D.D. Bromate formation in bromide-containing water through the cobalt-mediated activation of peroxymonosulfate. *Water Res.* **2015**, *83*, 132–140. [[CrossRef](#)]
50. Qian, Y.; Guo, X.; Zhang, Y.; Peng, Y.; Sun, P.; Huang, C.H.; Niu, J.; Zhou, X.; Crittenden, J.C. Perfluorooctanoic Acid Degradation Using UV-Persulfate Process: Modeling of the Degradation and Chlorate Formation. *Environ. Sci. Technol.* **2016**, *50*, 772–781. [[CrossRef](#)]
51. Sbardella, L.; Velo-Gala, I.; Comas, J.; Rodriguez-Roda Layret, I.; Fenu, A.; Gernjak, W. The impact of wastewater matrix on the degradation of pharmaceutically active compounds by oxidation processes including ultraviolet radiation and sulfate radicals. *J. Hazard. Mater.* **2019**, *380*, 120869. [[CrossRef](#)]
52. Jackson, A.; Gaffney, J.W.; Boulton, S. Subsurface Interactions of Fe(II) with Humic Acid or Landfill Leachate Do Not Control Subsequent Iron(III) (Hydr)oxide Production at the Surface. *Environ. Sci. Technol.* **2012**, *46*, 7543–7550. [[CrossRef](#)]
53. Feng, K.; Mu, S.; Bai, J.; Li, Q. Microwave-enhanced iron-carbon-activated hydrogen peroxide process for the advanced treatment of semi-aerobic aged refuse biofilter effluent. *Environ. Sci. Water Res. Technol.* **2021**, *7*, 2321–2334. [[CrossRef](#)]
54. Gu, Z.; Chen, W.; Li, Q.; Wang, Y.; Wu, C.; Zhang, A. Degradation of recalcitrant organics in landfill concentrated leachate by a microwave-activated peroxydisulfate process. *RSC Adv.* **2018**, *8*, 32461–32469. [[CrossRef](#)]
55. Guo, S.; Wang, Q.; Luo, C.; Yao, J.; Qiu, Z.; Li, Q. Hydroxyl radical-based and sulfate radical-based photocatalytic advanced oxidation processes for treatment of refractory organic matter in semi-aerobic aged refuse biofilter effluent arising from treating landfill leachate. *Chemosphere* **2020**, *243*, 125390. [[CrossRef](#)]
56. Chen, W.; Zhang, A.; Gu, Z.; Li, Q. Enhanced degradation of refractory organics in concentrated landfill leachate by Fe⁰/H₂O₂ coupled with microwave irradiation. *Chem. Eng. J.* **2018**, *354*, 680–691. [[CrossRef](#)]